Multifunctional hybrid silica nanoparticles based on [Mo Br]^2 phosphorescent nanosized clusters, magnetic γ-Fe O and plasmonic gold nanoparticles

Nicolas Nerambourg, Tangi Aubert, Chrystelle Neaime, Stéphane Cordier, Michel Mortier, Gilles Patriarche, Fabien Grasset

Multifunctionnal Hybrid Silica Nanoparticles Based on $[Mo_6Br_{14}]^{2-}$ Phosphorescent Nanosized Clusters, Magnetic γ-Fe_2O_3 and Plasmonic Gold Nanoparticles.

Nicolas Nerambourg[a,£*], Tangi Aubert[a,§], Chrystelle Neaime[a,d], Stéphane Cordier[a*], Michel Mortier[b], Gilles Patriarche[c] and, Fabien Grasset[a*]

[a] Solid State Chemistry and Materials group, UMR CNRS 6226, University of Rennes 1 263 av. du Général Leclerc, 35042 Rennes, France
[b] Institut de Recherche de Chimie Paris, CNRS – Chimie ParisTech, 11 rue Pierre et Marie Curie, 75005 Paris, France
[c] Laboratoire de Photonique et de Nanostructures (LPN-CNRS), Route de Nozay, 91460 Marcoussis, France
[d] Solid State Chemistry and Materials group, UMR CNRS 6226, INSA de Rennes 20 Avenue des Buttes de Coësmes, CS 70 839, 35 708 Rennes Cedex 7, France

[*] Contact Fax: +330223236799 Phone : +33 2 23 23 65 40
Email : nicolas.nerambourg@univ-lorraine.fr; stephane.cordier@univ-rennes1.fr; fabien.grasset@univ-rennes1.fr

[£] Present address: Struct & React Syst Mol Complexes, UMR CNRS 7565, University of Lorraine, F-54506 Vandoeuvre Les Nancy, France
[§] Present address: Department of Inorganic and Physical Chemistry, Ghent University, Belgium

Keywords: silica nanoparticles, metal atom clusters, luminescent nanoparticles, magnetic nanoparticles.

We report on the synthesis, characterization and photophysical study of new luminescent and magnetic hybrid silica nanoparticles. Our method is based on the co-encapsulation of single maghemite γ-Fe_2O_3 nanoparticles and luminescent molybdenum cluster units $[Mo_6Br^i_8Br^a_6]^{2-}$ through a water-in-oil (W/O) microemulsion technique. The as-prepared core-shell $[Cs_2Mo_6Br_{14}$-γ-$Fe_2O_3]$@SiO_2 nanoparticles (45-53 nm) possess a single magnetic core (6, 10.5

or 15 nm) and the cluster units are dispersed in the entire volume of the silica sphere. The $[Cs_2Mo_6Br_{14}$-γ$Fe_2O_3]@SiO_2$ nanoparticles have a perfect spherical shape with a good monodispersity and they display red and near-infrared (NIR) emission in water under UV excitation, whose intensity depends of the magnetic core size. The hybrid nanoparticles have been characterized by transmission electron microscopy (TEM), high annular angular dark field scanning transmission electron microscopy (HAADF-STEM), energy-dispersive X-ray spectroscopy (EDX), UV-Vis-NIR spectroscopy and magnetometer SQUID analysis. Small gold nanoparticles were successfully nucleated at the surface of the hybrid silica nanoparticles in order to add plasmonic properties.

Introduction

The design, synthesis and characterization of magnetic-luminescent nanoparticles (MLPs) have been more and more studied during the last decade. Indeed, the association of two distinct entities which independently possess magnetic and luminescent properties within a single nanoparticle is of great interest in the field of nanobiotechnology and nanomedicine. Such bimodal hybrid nanoparticles are particularly suitable for *in vitro* and *in vivo* bioimaging applications such as magnetic resonance imaging (MRI), fluorescence microscopy, cell tracking, magnetic separation and visualization, as well as for simultaneous diagnostic and therapeutic techniques, so called "Theranostic applications".[1]

Several approaches are described in the literature to develop such MLPs.[2, 3] For instance, many methods report the co-encapsulation of magnetic nanoparticles (MPs) with quantum dots (QDs), organic dyes, luminescent complexes in silica shells,[4-19] micelles,[20-23] or polymeric matrix.[24-26] Other approaches consisted in the direct assembly of QDs with MPs *via* specific functional groups,[27] electrostatic interaction,[28] nucleation of QDs at the surface of MPs,[29-31] or by layer-by-layer assembly.[18, 32] Similarly, the formation of MLPs was also reported through the functionalization of the MPs surface with luminescent organic ligands.[33-37] However, several issues still need to be tackled before fully controlled and reproducible syntheses of MLPs for biological applications can be achieved. This includes the size control of the final nano-object, the increase of their stability in solution, the optimization of the near-infrared (NIR) optical properties, the simplification of the experimental procedures, the increase of tissues penetration and the decrease of their cytotoxicity.

Here, we present a simple, versatile and efficient method based on silica nanoparticles incorporating MPs and luminescent nanosized $[Mo_6Br_{14}]^{2-}$ cluster units. These metal atom clusters exhibit a broad emission band in the red and NIR (550 to 900 nm, see the Supporting

Information for optical characterization) centered around 720 nm,[38] which is particularly interesting for biotechnology applications as it corresponds to a low absorption of human tissues at these wavelengths.[39] Moreover, they generate singlet oxygen under irradiation, what is of particular interest for photodynamic therapy (PDT).[40] Thus, thanks to the very good reproducibility of their synthesis in large amounts, $[Mo_6Br_{14}]^{2-}$ cluster units may represent a complementary alternative to traditional luminophores (organic dyes, QDs or lanthanide based nanocrystals) developed for bioimaging and biolabeling. Inorganic metal atom clusters salts as for instance $Cs_2Mo_6Br_{14}$ are synthesized by a solid state chemistry route at high temperature.[41] These compounds are built up from Cs cations and discrete $[Mo_6Br^i_8Br^a_6]^{2-}$ nanosized cluster units wherein the Mo_6 cluster is face-capped by eight inner bromine ligands (Br^i) and additionally bonded to six bromine apical ligands (Br^a) (see the Supporting Information Fig. S1). Owing to the ionic nature of the interaction between the cluster units and the cations, $Cs_2Mo_6Br_{14}$ solid state powder can be dispersed at molecular level in solution.[42] The $[Mo_6Br^i_8Br^a_6]^{2-}$ unit displays specific photochemical and redox properties leading to a relevant building block for the elaboration of hybrid nanomaterials.[43] For instance, tunable visible luminescent hybrid nanoparticles were recently obtained by associating $[Mo_6Br^i_8Br^a_6]^{2-}$ units along with ZnO nanocrystals in a silica matrix.[44] As reported earlier[42], owing to its good solubility in ethanol and acidic aqueous solutions, $Cs_2M_6Br_{14}$ is a relevant cluster precursor for the elaboration of luminescent silica nanoparticles by a water-in-oil (W/O) microemulsion technique. Compared to the Stöber process, the W/O microemulsion process is a powerful and versatile method for the synthesis of water-soluble and monodisperse multifunctional nanoparticles with complex architectures and below 50 nm in size. This robust method is highly reproducible and enables the encapsulation in a silica shell of all kind of water-soluble nanoparticles,[45-47] as well as hydrophobic nanoparticles such as gold / silver,[48] QDs,[49, 50] or Fe_3O_4.[10]

Moreover, small gold nanoparticles can be deposited on the surface of silica nanoparticles modified by amine-terminated silane molecules, allowing the preparation of gold nanoshells *via* seed-mediated growth.[51, 52] Gold nanoshells on silica nanoparticles were developed in the pioneer work of Halas in 1998.[53, 54] Thus, thanks to the strong absorption of the plasmon band in the visible region, gold nanoparticles and by extension gold nanoshells, can convert efficiently the absorbed light into heat, allowing the local destruction of tissues or cancer cells at their vicinity. These outstanding properties opened the way of new promising anti-cancer therapy, namely *Plasmonic PhotoThermal Therapy* (PPTT).[55] Consequently, the deposition of gold nanoparticles on the surface of silica nanoparticles incorporating MPs and $[Mo_6Br_{14}]^{2-}$ clusters units appeared very interesting.

We describe in this paper the co-encapsulation of γ-Fe_2O_3 MPs and luminescent molybdenum cluster units $[Mo_6Br^i_8Br^a_6]^{2-}$ in silica nanoparticles through a W/O microemulsion process. The synthesized nanoparticles (NPs), denoted $[Cs_2Mo_6Br_{14}$-γ-$Fe_2O_3]@SiO_2$, were fully characterized in terms of structural and optical properties. Although we already showed in the past the feasibility of co-encapsulating both MPs and cluster units in a silica matrix,[56] this paper focus in particular on the evolution of the luminescence properties of the MLPs as a function of the size of the magnetic core inside the nanoparticles. Compared to our previous work, this paper describes a very simple synthetic process to obtain magnetic and luminescent silica nanoparticles with a tunable magnetic core size and with a perfect morphology. In addition, for even more advanced biotechnological applications, small gold NPs were *in situ* nucleated on the surface of the MLPs to form magnetic, plasmonic and ideally luminescent $[Cs_2Mo_6Br_{14}$-γ-$Fe_2O_3]@SiO_2@Au$ hybrid nanoparticles.

Experimental section

Characterization of Materials

Absorbance measurements of the hybrid nanoparticles suspension were recorded with a Lambda 35 PerkinElmer UV-visible spectrophotometer. Luminescence properties were investigated with a Fluorolog-3 fluorescence spectrophotometer (FL3-22, Horiba Jobin Yvon).

Time-resolved photoluminescence measurements were performed with a device using a charge-coupled device (CCD) camera placed at the exit slit of a 0.25 m Jobin Yvon monochromator. 8 ns excitation pulses were provided by an optical parametric oscillator (OPO) optically pumped by the third harmonic of a Nd:YAG Q-switched laser.

Transmission electron microscopy (TEM) samples were performed at the Microscopy Rennes Imaging Center MRic-TEM (UMS 3480). Samples were observed with a JEOL 1400 TEM at 120 KV provided of GATAN orius camera (4k×2k pixels).

The distribution of the cluster units inside the silica matrix was observed by high annular angular dark field scanning transmission electron microscopy (HAADF-STEM) using a JEOL 2200FS Cs corrected TEM/STEM operating at 200 kV and equipped with an EDX system. The probe size is 0.12 nm (FWHM) with a current of 150 pA. The half-angle of convergence of the probe is 30 mrad. HAADF detector (half)angles: 100 mrad (inner) to 170 mrad (outter). We have used amorphous silicon nitride membranes (30 nm thick) to disperse the nanoparticles.

Synthesis of γ-Fe_2O_3 NPs

Magnetic γ-Fe_2O_3 nanoparticles were prepared according to Sun's method,[57] which allows the synthesis of stable, monodisperse and hydrophobic iron oxide NPs capped with organic

ligands. The size of the MPs can be tuned easily between 4 and 20 nm through a seeded-growth process. Although this method was initially reported for the synthesis of magnetite (Fe_3O_4) NPs, they gradually oxidize under ambient air to form maghemite (γ-Fe_2O_3) NPs, as confirmed by Mossbauer spectroscopy (data not shown). Thus, in the following we will consider the magnetic nanoparticles as γ-Fe_2O_3 and not Fe_3O_4. Magnetic nanoparticles of 6, 10.5 and 15 nm in size were synthesized (Fig. 1, see the Supporting Information Fig. S3 for size distributions). To facilitate the encapsulation process in the silica matrix, the as-prepared hydrophobic γ-Fe_2O_3 NPs were transferred in water by a peptization process, which consists in several washings of the MPs with HNO_3 2 M in order to remove the hydrophobic native capping ligands (see the Supporting Information for detailed procedure).[58] Afterward, the surface of the MPs is covered with positive charges, allowing a relatively good dispersion of the MPs in water.

Synthesis of $[Cs_2Mo_6Br_{14}$-γ-$Fe_2O_3]@SiO_2$ NPs

The bi-modal magnetic and luminescent $[Cs_2Mo_6Br_{14}$-γ-$Fe_2O_3]@SiO_2$ NPs were prepared by a W/O microemulsion technique. Briefly, a W/O microemulsion consists in aqueous nanodroplets dispersed in an oil phase and stabilized at their interface by surfactant molecules. These nanodroplets, also called inverted micelles, constitute nano-reactors suitable for the synthesis of silica nanoparticles.[59] The crucial point of the W/O microemulsion technique is the stability of the system, especially when different kind of species have to be embedded in the silica nanoparticles. It appears evident in our case that aggregation of cluster units, or γ-Fe_2O_3 MPs, or strong interactions between cluster units and γ-Fe_2O_3 MPs during the microemulsion, could cause the destabilization of the system. Consequently, the concentration of the different species, as well as their order of addition in the microemulsion are

fundamental key points. In our synthesis, *n*-heptane was used as the oil phase, Brij30 as the surfactant, tetraethoxysilane (TEOS) as the silica precursor and the aqueous phase was actually constituted of both the γ-Fe_2O_3 and cluster solutions. First the microemulsion was created by adding slowly an aqueous suspension of γ-Fe_2O_3 MPs (~ 13 mg in 750 µL of water) to a mixture of heptane (23.5 mL) and Brij30 (7.5 mL). After a perfect homogeneity of the microemulsion was reached, a cluster sol was slowly added. The cluster sol was obtained by the solubilization of the cluster compound in a EtOH:H_2O mixture (1:1 volume ratio) (see the Supporting Information for detailed procedure). Afterward, an aqueous ammonia solution (28%, 200 µL) was added. Once the microemulsion became clear and transparent, TEOS (1 mL) was added and the mixture was left under magnetic stirring for 72h. The microemulsion was then destabilized by addition of a large volume of ethanol (40 mL) and the NPs were purified by several precipitation / resuspension cycles by centrifugation to remove surfactant molecules and aggregates formed during the microemulsion. In this work, [$Cs_2Mo_6Br_{14}$-γFe_2O_3]@SiO_2 nanoparticles were synthesized with magnetic cores of either 6, 10.5 or 15 nm in size. [$Cs_2Mo_6Br_{14}$]@SiO_2 without any magnetic core were also synthesized for comparative studies (see the Supporting Information Fig. S4 for size distributions).

Synthesis of [$Cs_2Mo_6Br_{14}$-γFe_2O_3]@SiO_2@Au nanoparticles

[$Cs_2Mo_6Br_{14}$-γFe_2O_3]@SiO_2@Au nanoparticles were prepared as follow: an aqueous suspension of [$Cs_2Mo_6Br_{14}$-γFe_2O_3]@SiO_2 NPs with magnetic cores of 10.5 nm (4 mL, 12 mg/mL) was adjusted to pH 12 with a solution of NH_4OH 28%. The suspension was slowly added to a solution of gold salt (13.6 mg in 2 mL of water) and left under stirring overnight. The suspension was then purified by 3 centrifugation / resuspension (10000*g*) cycles in water and the precipitate was finally suspended in 10 mL of water. The sample was placed few

centimeters below a classical portable UV light (365 nm, 6W) and left under illumination during 17h to form $[Cs_2Mo_6Br_{14}$-γ$Fe_2O_3]@SiO_2$@Au nanoparticles.

Results and discussion

Nanoparticles Morphology

Fig. 1 shows the TEM images of the MPs of the three different sizes and the corresponding $[Cs_2Mo_6Br_{14}$-γ$Fe_2O_3]@SiO_2$ nanoparticles. These latter ones present a perfect spherical and monodisperse morphology with an average diameter of 53, 50 and 45 nm for magnetic core size of 15, 10.5 and 6 nm respectively. The magnetic cores are always localized in the center of the spherical silica matrix and there are almost no empty silica beads. The thickness of the silica shell around the MPs is more or less the same (18-20 nm) independently of the size of the MPs. This means that the silica thickness is controlled exclusively by the amount of TEOS and the condensation time of the corresponding hydrolyzed molecules. These parameters were kept constant for all the syntheses and the experimental procedure is perfectly reproducible, leading to the same size and monodispersity from one batch to another. Other experiments were carried out to encapsulate several MPs by increasing the MPs concentration. The result was a total destabilization of the microemulsion.

The $[Cs_2Mo_6Br_{14}$-γ$Fe_2O_3]@SiO_2$ nanoparticles were also observed by high annular angular dark field scanning transmission electron microscopy (HAADF-STEM) which is the only suitable tool to visualize the cluster units within the silica matrix (Fig. 2). Indeed, by detecting electrons scattered at high angles this technique provides Z-contrast images as atoms with higher atomic numbers will scatter more electrons at high angle than atoms with lower atomic numbers. Thus, thanks to the large difference in atomic numbers between the cluster core and

Si or O from the silica matrix and the high spatial resolution of the STEM, it was possible to visualize the cluster units inside the nanoparticles. In Fig. 2, although the magnetic cores are still visible in the center of the nanoparticles, the cluster units also appear as bright spots, dispersed over the entire volume of the nanoparticles. In order to confirm unambiguously that these bright spots correspond to the cluster units and not to potential irregular spots from the STEM images, EDX elemental analyses were performed at different locations of the MLPs (Fig. 3). The resulting chemical composition clearly indicates the presence of molybdenum in the entire volume of the silica matrix, whereas iron is only detected in the center of the particles where the γ-Fe_2O_3 nanoparticles are localized.

The HAADF-STEM images (Fig. 2) also evidence that a certain amount of the clusters used for the synthesis of the MLPs are located at the surface of the nanoparticles. Cluster units located close to the dispersing medium are potentially useful. Indeed, upon irradiation cluster units can interact with molecular oxygen and relax through the formation of singlet oxygen, which is of particular interest for PDT applications.[60]

Photophysical properties

The effect of the size of the magnetic core on the photophysical properties of the synthesized MLPs was investigated in details. The absorption spectra of $[Cs_2Mo_6Br_{14}]@SiO_2$ nanoparticles and those of $[Cs_2Mo_6Br_{14}$-γ-$Fe_2O_3]@SiO_2$ nanoparticles with different core sizes are shown in Fig. 4. Spectra were normalized at 215 nm where the corresponding large absorption band is due to the absorption of the cluster units. The presence of the magnetic nanoparticles does not cause any shift on the absorption bands of the cluster units. Nevertheless, the influence of the MPs is visible by an increase of the absorption between 225 and 500 nm as the size of the magnetic core increases. Indeed, as illustrated in the inset of Fig.

4 the absorption feature of γ-Fe_2O_3 nanoparticles measured separately in cyclohexane after their synthesis increases with their size. The absorption spectra of the MLPs are consequently the addition of the absorption of the cluster units and the MPs, without any influence of one on the other.

As already mentioned, the emission of Mo_6 cluster units is generally quenched in solution due to the presence of molecular oxygen and through the formation of singlet oxygen. We already demonstrated that embedding the cluster units in a silica matrix prevents to some extend this process, the silica acting as a protective barrier against the diffusion of molecular oxygen. [61] The emission spectra of $[Cs_2Mo_6Br_{14}]@SiO_2$ nanoparticles and those of $[Cs_2Mo_6Br_{14}$-γ$Fe_2O_3]@SiO_2$ nanoparticles in water recorded before and after deoxygenation are shown in Fig. 5 and data are gathered in Table 1. All the samples were adjusted to the same concentration of molybdenum clusters as estimated by inductively coupled plasma mass spectrometry analyses (ICP-MS).

On one hand, the quenching effect of the oxygen is obvious; the luminescence intensity of every sample decreases by 30 to 38% in the presence of oxygen, as compared to the same sample without oxygen (Table 1). This means that the silica shell does not protect totally the clusters from the effect of oxygen, which can diffuse through the silica pores. In addition, we showed that a certain amount of the cluster units were located in the outer part of the silica nanoparticles or even at their surface. These cluster units are therefore not protected from oxygen molecules and consequently their luminescence is fully quenched.

On the other hand, the size of the magnetic core plays an important role on the luminescence intensity of the clusters, even if their presence in the vicinity of the clusters within the silica matrix does not cause any observable shift on the maximum of the emission wavelength, centered around 720 nm. The emission spectra of the samples after deoxygenation suggest

that the smallest MPs do not influence the luminescence intensity of the clusters, while it considerably decreases in the presence of the 10.5 and 15 nm MPs.

In order to quantify the size effect of the magnetic core on the emission intensity of the clusters (Table 1), the luminescence of $[Cs_2Mo_6Br_{14}]@SiO_2$ in degassed solution was taken as reference and all samples were adjusted to the same concentration of clusters. The partial inhibition of the emission due to the magnetic core size is around 50% and 60% for respectively 10.5 and 15 nm MPs. Clusters are not affected, or to a lesser extent, by the 6 nm MPs. Their luminescence intensity corresponds almost exactly to the intensity of $[Cs_2Mo_6Br_{14}]@SiO_2$ after deoxygenation

The quenching of luminescent species (organic dyes or QDs) caused by the proximity of magnetic nanoparticles is well known[2] but as far as we know, it is the first time that the influence of the size of single magnetic nanoparticles on the photophysical properties of luminescent entities is investigated. This quenching is generally ascribed to non-radiative transfer or to the strong absorption of the incident light by the iron oxide nanoparticles. Regarding the absorption spectra of the iron oxide nanoparticles in the range of 300-700 nm (inset Fig. 3), it appears obvious that the excitation light at 450 nm is stronger absorbed as the size of the MPs is bigger. Less photon are consequently absorbed by the cluster units located in the vicinity of the biggest iron oxide nanoparticles, resulting in a decrease of the emission intensity.

Time correlated single photon counting (TCSPC) experiments were carried out at room temperature, in water and in aerated conditions on $[Cs_2Mo_6Br_{14}]@SiO_2$ and $[Cs_2Mo_6Br_{14}$-$\gamma Fe_2O_3]@SiO_2$, in order to evaluate the influence of the magnetic core size on the clusters lifetime. Samples were excited at λ_{exc} = 450 nm and the luminescence observed at λ_{obs} = 700 nm. Data are summarized in Table 2. For each sample, three lifetimes were obtained and are composed of a long (100 – 90 µs), an intermediate (50 – 30 µs) and a short component (20 –

8.5 µs). All these lifetimes are coherent to each other except the third lifetime of $[Cs_2Mo_6Br_{14}$-γ$Fe_2O_3]@SiO_2$ containing 10.5 nm magnetic core (20 µs against 8.5-10 µs for the others). However, the fitting method manifests not negligible incertitude due to the large number of parameters (6 different parameters). Lifetime measurements on $Cs_2[Mo_6Br_{14}]@SiO_2$ were previously reported on solid state conditions[42, 44] and were composed of a long component (40 µs) attributed to the phosphorescence of the $[Mo_6Br_{14}]^{2-}$ cluster units and a short component (~ 2 µs) attributed to energy transfers between the cluster units themselves or with the silica matrix. These values differ from those presented in this study because of the different experimental conditions (solid state condition *vs.* suspension condition).

Furthermore, the deconvolution of the emission spectrum of $[Mo_6Br_{14}]^{2-}$ cluster units shows two distinct emission bands corresponding to different excited states.[44, 62] If we take into account what has been said and if we consider the potential interactions of the different entities (interactions between MLPs to each other, between clusters to each other, between clusters and the silica matrix and finally between clusters and γ-Fe_2O_3), a relevant attribution of the three obtained lifetimes is particularly tricky. Other TSPC experiments were performed by changing λ_{obs} (λ_{obs} = 675 and 770 nm) without giving fruitful information. New studies concerning the different excited states involved in the deactivation process of the $[Mo_6Br_{14}]^{2-}$ are under investigations. However, on the basis of the measured lifetimes reported in table 2, we can assume that the magnetic cores do not have a significant influence on the lifetimes of the cluster units.

Magnetic properties

The magnetic properties of the different MLPs were studied by using a superconducting quantum interference device (SQUID). Hysteresis loops of the samples were recorded at temperatures of 2 and 300 K (Fig. 6). $[Cs_2Mo_6Br_{14}$-γ-$Fe_2O_3]@SiO_2$ nanoparticles exhibit no coercivity (*Hc*) and remanence at 300 K, meaning that the magnetic nanoparticles maintain their superparamagnetic property in the silica matrix. The saturation magnetization (*Ms)* values were 44, 38 and 26 emu g^{-1} for MLPs incorporating respectively 15, 10.5 and 6 nm sized γ-Fe_2O_3 MPs. These values are slightly lower than those of the MPs before their encapsulation in silica, which was found to be 62, 64 and 45 emu g^{-1} respectively for 15, 10.5 and 6 nm sized γ-Fe_2O_3 MPs (Fig. S5). The decrease of *Ms* of γ-Fe_2O_3 embedded in silica can be explained by taking into account the diamagnetic contribution of the thick silica shell surrounding the magnetic cores.[18] The decrease of *Ms* values with the size of the magnetic nanoparticles is due to the fact that *Ms* depends directly of the volume of the nanoparticles.[63] At 2 K, the core/shell nanoparticles exhibited ferrimagnetic characteristics, including coercivity (*Hc* = 160 and 135 Oe for respectively 15/10.5 and 6 nm sized γ-Fe_2O_3 MPs) and remanence. The coercivity for the corresponding γ-Fe_2O_3 MPs were *Hc* = 300, 225 and 170 Oe for diameters of 15, 10.5 and 6 nm. The corresponding *Ms* values were 104, 102 and 84 from the biggest to the smallest magnetic core. These values are higher at low temperature due to thermal fluctuations which occur at higher temperature.

The temperature dependence of the magnetization of the MLPs was measured in zerofield-cooled (ZFC) and field-cooled (FC) modes within an applied field of 50 Oe (Fig. 7). In ZFC mode, the magnetization of the MLPs exhibits a broad maximum at T_{max} = 26, 36 and 47 K (for respectively 6, 10.5 and 15 nm diameter core) which is characteristic when freezing superparamagnetic nanoparticles, due to magnetic anisotropy. It is generally assumed that the temperature of this maximum depends on the average particle size and increases with the size

of the particles. On cooling, the FC magnetization values are identical to that of ZFC magnetization at higher temperatures. Such behavior is characteristic of superparamagnetism and is due to the progressive blocking of the magnetization of smaller and smaller particles when temperature is decreasing. The temperature at which the ZFC and the FC curves get separated indicates the onset of the blocking for the largest γ-Fe_2O_3 nanoparticles, while the maximum temperature in the ZFC curve (T_{max}) can be related to the blocking temperature with the average volume.

Toward plasmonic and magnetic hybrid nanoparticles

Gold nanoparticles were successfully generated on the surface of $[Cs_2Mo_6Br_{14}$-γ-$Fe_2O_3]@SiO_2$ (magnetic core: 10.5 nm) by the direct nucleation of gold ions immobilized on their surfaces. The goal was to obtain a single hybrid system which possesses magnetic and plasmonic properties. The main difficulty in such system is to preserve the luminescence of the cluster units, which is already affected by the presence of the MPs.

It is well known that the interaction between gold nanoparticles and luminescent species leads to a strong quenching of the luminescence properties,[64] even if an enhancement of these properties is observed in some cases.[65] The key of the effect, quenching or exaltation, is mainly due to the distance between the metallic center and the luminescent entities[66], as well as the position of the plasmon band compared to the emission band of the luminophore.[67]

Our strategy was to develop a very easy and elegant method minimizing the number of synthetic steps, which are in the most of the cases very delicate to reproduce. In a first step,

Au^{3+} ions are immobilized at the surface of $[Cs_2Mo_6Br_{14}$-γ$Fe_2O_3]@SiO_2$ by adding a solution of $HAuCl_4 \cdot 3H_2O$ to a suspension of $[Mo_6Br_{14}$-γ$Fe_2O_3]@SiO_2$ adjusted to pH 12.

The pH of the suspension plays a crucial role on the adsorption of Au^{3+} ions on the silica surface. Indeed, without modification of the pH of the MLPs suspension in water (~ pH 9), Au^{3+} ions are not immobilized on the silica surface. After a purification step by centrifugation, the supernatant was yellow, typical color of the gold salt solution, and turned instantaneously to black when a diluted solution of $NaBH_4$ was added, characteristic of the nucleation and aggregation of a concentrated gold ions solution. The color of the resuspended solid remained unchanged after addition of $NaBH_4$, revealing the absence of Au^{3+} ions. The opposite was observed at pH 12; the supernatant was colorless while the resuspended solid turned black after the addition of $NaBH_4$. When added to a colloidal suspension of $[Mo_6Br_{14}$-γ$Fe_2O_3]@SiO_2$ at pH 12, Au^{3+} ions formed specific complexes with $Si\text{-}O^-$ groups present at the surface of the silica nanoparticles.

After immobilization of Au^{3+} ions on the surface of $[Cs_2Mo_6Br_{14}$-γ$Fe_2O_3]@SiO_2$ nanoparticles, the sample was illuminated with a UV light source (λ_{exc} = 365nm, 6W) in order to nucleate softly the Au^{3+} ions. The use of reductant like $NaBH_4$ is not appropriated and lead to inhomogeneous formation of aggregates or different sizes of gold NPs (Fig. S6).

Fig. 8 reports the time-evolution of the absorption of $[Cs_2Mo_6Br_{14}$-γ$Fe_2O_3]@SiO_2@Au^{3+}$ under UV light illumination during 17h, as well as the corresponding photos of the suspension. During the irradiation, the intensity of the absorbance decreases between 250 and 500 nm while it increases around 550 nm after 15h. This feature related to the disappearance of the gold salt with the formation of gold NPs. The shape of the plasmon band is slightly asymmetric, its intensity very weak and centered around 550 nm. The color of the suspension turned progressively from yellow to dark gray during the illumination experiment. It appears

from Fig. 8 that a fraction of gold metal generated under the irradiation process stuck to the sides of the vial. This is due to the formation of large gold aggregates which stuck on the vial because of its horizontal position during the irradiation. These aggregates are eliminated during the purification by a centrifugation step.

After purification, TEM analysis of $[Cs_2Mo_6Br_{14}\text{-}\gamma Fe_2O_3]@SiO_2@Au$ reveals a homogeneous distribution of very small gold NPs (< 2 nm) all over the surface of the silica nanoparticles (Fig. 9). The small size of the gold NPs is coherent with the very weak intensity of the plasmon band showed in Fig. 8. However, for very well uniform and monodisperse 2 nm gold nanoparticles, the plasmon band should be nearly inexistent and centered around 500-520 nm.[68, 69] The intensity of the plasmon band as well as its position are probably due to the contribution of bigger gold nanoparticles around 10 nm and / or aggregates which are present on the surface of the silica (see the Supporting Information Fig. S7). All these different gold species contribute to the unsymmetrical shape and to the intensity of the plasmon band and so to the gray color of the suspension but are not at all representative of the major morphology of the sample.

Conclusion

In conclusion, we successfully elaborated superparamagnetic and luminescent silica nanoparticles $[Cs_2Mo_6Br_{14}\text{-}\gamma Fe_2O_3]@SiO_2$ emitting in the red region of the visible spectrum. All the MLPs are well spherical with a good monodispersity and have a mean diameter inferior to 55 nm. The luminescence intensity of the MLPs is quenched by 50 to 60% for magnetic core sizes of 10.5 or 15 nm. Interestingly, the luminescence intensity is not affected by the smallest MPs (6 nm). Owing to their bi-modal properties and their small sizes, these nanoparticles are well suitable for biomedical applications. Indeed it is well known that the

surface of the silica nanoparticles can be modified easily by organosilane molecules for the grafting of biomolecules of interest. Finally we succeeded in obtaining a third functionality by nucleating small 2 nm gold nanoparticles all over the surface of the magnetic-fluorescent silica nanoparticles in a very easy and reproducible way. Such multifunctional nanoparticles constitute interesting candidates for theranostic applications.

Acknowledgements

This work was supported by the University of Rennes 1, CNRS, ANR (Project CLUSTOP 2011 BS08 013 01). The authors thank Agnès Burel for technical assistance and fruitful discussions concerning the TEM experiments (Service of Transmission Electron Microscopy, University Rennes 1).

References

1. J. L. Vivero-Escoto, R. C. Huxford-Phillips and W. Lin, *Chemical Society Reviews*, 2012, **41**, 2673-2685.
2. S. A. Corr, Y. P. Rakovich and Y. K. Gun'ko, *Nanoscale Res. Lett.*, 2008, **3**, 87-104.
3. R. Kas, E. Sevinc, U. Topal and H. Y. Acar, *Journal of Physical Chemistry C*, 2010, **114**, 7758-7766.
4. D. K. Yi, S. T. Selvan, S. S. Lee, G. C. Papaefthymiou, D. Kundaliya and J. Y. Ying, *Journal of the American Chemical Society*, 2005, **127**, 4990-4991.
5. R. He, X. G. You, J. Shao, F. Gao, B. F. Pan and D. X. Cui, *Nanotechnology*, 2007, **18**.
6. T. M. Ruhland, P. M. Reichstein, A. P. Majewski, A. Walther and A. H. E. Muller, *Journal of Colloid and Interface Science*, 2012, **374**, 45-53.
7. F. Wang, X. Chen, Z. Zhao, S. Tang, X. Huang, C. Lin, C. Cai and N. Zheng, *Journal of Materials Chemistry*, 2011, **21**, 11244-11252.
8. J. Kim, J. E. Lee, J. Lee, J. H. Yu, B. C. Kim, K. An, Y. Hwang, C.-H. Shin, J.-G. Park, J. Kim and T. Hyeon, *Journal of the American Chemical Society*, 2005, **128**, 688-689.
9. J. Kim, H. S. Kim, N. Lee, T. Kim, H. Kim, T. Yu, I. C. Song, W. K. Moon and T. Hyeon, *Angewandte Chemie International Edition*, 2008, **47**, 8438-8441.
10. C. W. Lu, Y. Hung, J. K. Hsiao, M. Yao, T. H. Chung, Y. S. Lin, S. H. Wu, S. C. Hsu, H. M. Liu, C. Y. Mou, C. S. Yang, D. M. Huang and Y. C. Chen, *Nano Letters*, 2007, **7**, 149-154.

11. N. Chekina, D. Horak, P. Jendelova, M. Trchova, M. J. Benes, M. Hruby, V. Herynek, K. Turnovcova and E. Sykova, *Journal of Materials Chemistry*, 2011, **21**, 7630-7639.
12. G. N. Wang, C. Wang, W. C. Dou, Q. Ma, P. F. Yuan and X. G. Su, *Journal of Fluorescence*, 2009, **19**, 939-946.
13. C. W. Lai, Y. H. Wang, C. H. Lai, M. J. Yang, C. Y. Chen, P. T. Chou, C. S. Chan, Y. Chi, Y. C. Chen and J. K. Hsiao, *Small*, 2008, **4**, 218-224.
14. A. Abou-Hassan, R. Bazzi and V. Cabuil, *Angewandte Chemie-International Edition*, 2009, **48**, 7180-7183.
15. A. Lapresta-Fernandez, T. Doussineau, S. Dutz, F. Steiniger, A. J. Moro and G. J. Mohr, *Nanotechnology*, 2011, **22**.
16. B. B. Zhang, B. D. Chen, Y. L. Wang, F. F. Guo, Z. Q. Li and D. L. Shi, *Journal of Colloid and Interface Science*, 2011, **353**, 426-432.
17. D. Müller-Schulte, T. Schmitz-Rode and P. Borm, *Journal of Magnetism and Magnetic Materials*, 2005, **293**, 135-143.
18. V. Salgueiriño-Maceira, M. A. Correa-Duarte, M. Spasova, L. M. Liz-Marzán and M. Farle, *Advanced Functional Materials*, 2006, **16**, 509-514.
19. N. Insin, J. B. Tracy, H. Lee, J. P. Zimmer, R. M. Westervelt and M. G. Bawendi, *ACS Nano*, 2008, **2**, 197-202.
20. V. Roullier, F. Grasset, F. Boulmedais, F. Artzner, O. Cador and V. Marchi-Artzner, *Chemistry of Materials*, 2008, **20**, 6657-6665.
21. A. R. Herdt, B.-S. Kim and T. A. Taton, *Bioconjugate Chemistry*, 2006, **18**, 183-189.
22. G. A. F. van Tilborg, W. J. M. Mulder, N. Deckers, G. Storm, C. P. M. Reutelingsperger, G. J. Strijkers and K. Nicolay, *Bioconjugate Chemistry*, 2006, **17**, 741-749.
23. K. Vuu, J. Xie, M. A. McDonald, M. Bernardo, F. Hunter, Y. Zhang, K. Li, M. Bednarski and S. Guccione, *Bioconjugate Chemistry*, 2005, **16**, 995-999.
24. N. Gaponik, I. L. Radtchenko, G. B. Sukhorukov and A. L. Rogach, *Langmuir*, 2004, **20**, 1449-1452.
25. Y. Wu, M. Chu, B. Shi and Z. Li, *Applied Biochemistry and Biotechnology*, 2011, **163**, 813-825.
26. R. Di Corato, P. Piacenza, M. Musaro, R. Buonsanti, P. D. Cozzoli, M. Zambianchi, G. Barbarella, R. Cingolani, L. Manna and T. Pellegrino, *Macromol. Biosci.*, 2009, **9**, 952-958.
27. D. S. Wang, J. B. He, N. Rosenzweig and Z. Rosenzweig, *Nano Letters*, 2004, **4**, 409-413.
28. B. Liu, W. Xie, D. Wang, W. Huang, M. Yu and A. Yao, *Materials Letters*, 2008, **62**, 3014-3017.
29. X. Lu, R. Jiang, Q. Fan, L. Zhang, H. Zhang, M. Yang, Y. Ma, L. Wang and W. Huang, *Journal of Materials Chemistry*, 2012, **22**, 6965-6973.
30. R. Fu, W. Wang, R. Han and K. Chen, *Materials Letters*, 2008, **62**, 4066-4068.
31. X. Liu, Q. Hu, X. Zhang, Z. Fang and Q. Wang, *The Journal of Physical Chemistry C*, 2008, **112**, 12728-12735.
32. X. Hong, J. Li, M. Wang, J. Xu, W. Guo, J. Li, Y. Bai and T. Li, *Chemistry of Materials*, 2004, **16**, 4022-4027.
33. H. Gu, K. Xu, Z. Yang, C. K. Chang and B. Xu, *Chemical Communications*, 2005, 4270-4272.
34. Z. C. Liu, B. Li, B. D. Wang, Z. Y. Yang, Q. Wang, T. R. Li, D. D. Qin, Y. Li, M. F. Wang and M. H. Yan, *Dalton Transactions*, 2012, **41**, 8723-8728.
35. P. Xi, K. Cheng, X. Sun, Z. Zeng and S. Sun, *Chemical Communications*, 2012, **48**, 2952-2954.
36. P. Xi, K. Cheng, X. Sun, Z. Zeng and S. Sun, *Journal of Materials Chemistry*, 2011, **21**, 11464-11467.
37. F. Grasset, S. Mornet, A. Demourgues, J. Portier, J. Bonnet, A. Vekris and E. Duguet, *Journal of Magnetism and Magnetic Materials*, 2001, **234**, 409-418.
38. A. W. Maverick, J. S. Najdzionek, D. MacKenzie, D. G. Nocera and H. B. Gray, *Journal of the American Chemical Society*, 1983, **105**, 1878-1882.
39. C. H. Contag and B. D. Ross, *Journal of Magnetic Resonance Imaging*, 2002, **16**, 378-387.

40. L. Gao, M. A. Peay and T. G. Gray, *Chemistry of Materials*, 2010, **22**, 6240-6245.
41. K. Kirakci, S. Cordier and C. Perrin, *Zeitschrift Fur Anorganische Und Allgemeine Chemie*, 2005, **631**, 411-416.
42. F. Grasset, F. Dorson, S. Cordier, Y. Molard, C. Perrin, A. M. Marie, T. Sasaki, H. Haneda, Y. Bando and M. Mortier, *Advanced Materials*, 2008, **20**, 143-+.
43. S. Cordier, F. Dorson, F. Grasset, Y. Molard, B. Fabre, H. Haneda, T. Sasaki, M. Mortier, S. Ababou-Girard and C. Perrin, *Journal of Cluster Science*, 2009, **20**, 9-21.
44. T. Aubert, N. Nerambourg, N. Saito, H. Haneda, N. Ohashi, M. Mortier, S. Cordier and F. Grasset, *Particle & Particle Systems Characterization*, 2013, **30**, 90-95.
45. T. Aubert, F. Cabello Hurtado, M.A. Esnault, C. Neaime, D. Lebret-Chauvel, S. Jeanne, P. Pellen, C. Roiland, L. Le Polles, N. Saito, K. Kimoto, H. Haneda, N. Ohashi, F. Grasset, S. Cordier, *J. Phys. Chem. C,* 2013, **117**, 20154−20163.
46. T. Aubert, F. Grasset, S. Mornet, E. Duguet, O. Cador, S. Cordier, Y. Molard, V. Demange, M. Mortier and H. Haneda, *Journal of Colloid and Interface Science*, 2010, **341**, 201-208.
47. V. Maurice, I. Rivolta, J. Vincent, O. Raccurt, J-N. Rouzaud, G. Miserrochi, E. Doris, C. Reynaud, N. Herlin-Boime, J Nanopart Res, 2012, 14:697
48. Y. Han, J. Jiang, S. S. Lee and J. Y. Ying, *Langmuir*, 2008, **24**, 5842-5848.
49. R. Koole, M. M. van Schooneveld, J. Hilhorst, C. de Mello Donegá, D. C. . Hart, A. van Blaaderen, D. Vanmaekelbergh and A. Meijerink, *Chemistry of Materials*, 2008, **20**, 2503-2512.
50. M. Darbandi, R. Thomann and T. Nann, *Chemistry of Materials*, 2005, **17**, 5720-5725.
51. J. H. Kim, W. W. Bryan and T. R. Lee, *Langmuir*, 2008, **24**, 11147-11152.
52. T. Pham, J. B. Jackson, N. J. Halas and T. R. Lee, *Langmuir*, 2002, **18**, 4915-4920.
53. S. L. Westcott, S. J. Oldenburg, T. R. Lee and N. J. Halas, *Langmuir*, 1998, **14**, 5396-5401.
54. S. J. Oldenburg, R. D. Averitt, S. L. Westcott and N. J. Halas, *Chemical Physics Letters*, 1998, **288**, 243-247.
55. X. H. Huang, P. K. Jain, I. H. El-Sayed and M. A. El-Sayed, *Lasers in Medical Science*, 2008, **23**, 217-228.
56. F. Grasset, F. Dorson, Y. Molard, S. Cordier, V. Demange, C. Perrin, V. Marchi-Artzner and H. Haneda, *Chemical Communications*, 2008, 4729-4731.
57. S. H. Sun, H. Zeng, D. B. Robinson, S. Raoux, P. M. Rice, S. X. Wang and G. X. Li, *Journal of the American Chemical Society*, 2004, **126**, 273-279.
58. O. Cador, F. Grasset, H. Haneda and J. Etourneau, *Journal of Magnetism and Magnetic Materials*, 2004, **268**, 232-236.
59. M. A. Lopez-Quintela, *Current Opinion in Colloid & Interface Science*, 2003, **8**, 137-144.
60. J. A. Jackson, C. Turro, M. D. Newsham and D. G. Nocera, *The Journal of Physical Chemistry*, 1990, **94**, 4500-4507.
61. T. Aubert, A. Y. Ledneva, F. Grasset, K. Kimoto, N. G. Naumov, Y. Molard, N. Saito, H. Haneda and S. Cordier, *Langmuir*, 2010, **26**, 18512-18518.
62. H. Miki, T. Ikeyama, Y. Sasaki and T. Azumi, *Journal of Physical Chemistry*, 1992, **96**, 3236-3239.
63. C. Caizer and I. Hrianca, *Annalen der physik*, 2003, **12**, 115-122.
64. N. Nerambourg, M. H. V. Werts, M. Charlot and M. Blanchard-Desce, *Langmuir*, 2007, **23**, 5563-5570.
65. H. Chen, T. Ming, L. Zhao, F. Wang, L.-D. Sun, J. Wang and C.-H. Yan, *Nano Today*, 2010, **5**, 494-505.
66. G. Schneider, G. Decher, N. Nerambourg, R. Praho, M. H. V. Werts and M. Blanchard-Desce, *Nano Letters*, 2006, **6**, 530-536.
67. M. A. Noginov, G. Zhu, A. M. Belgrave, R. Bakker, V. M. Shalaev, E. E. Narimanov, S. Stout, E. Herz, T. Suteewong and U. Wiesner, *Nature*, 2009, **460**, 1110-U1168.

68. M. M. Alvarez, J. T. Khoury, T. G. Schaaff, M. N. Shafigullin, I. Vezmar and R. L. Whetten, *Journal of Physical Chemistry B*, 1997, **101**, 3706-3712.
69. A. Henglein, *Langmuir*, 1999, **15**, 6738-6744.

Multifunctionnal Hybrid Silica Nanoparticles Based on $[Mo_6Br_{14}]^{2-}$ Phosphorescent Nanosized Clusters, Magnetic γ-Fe_2O_3 and Plasmonic Gold Nanoparticles.

Nicolas Nerambourg, Tangi Aubert, Chrystelle Neaime, Stéphane Cordier, Michel Mortier, Gilles Patriarche and, Fabien Grasset

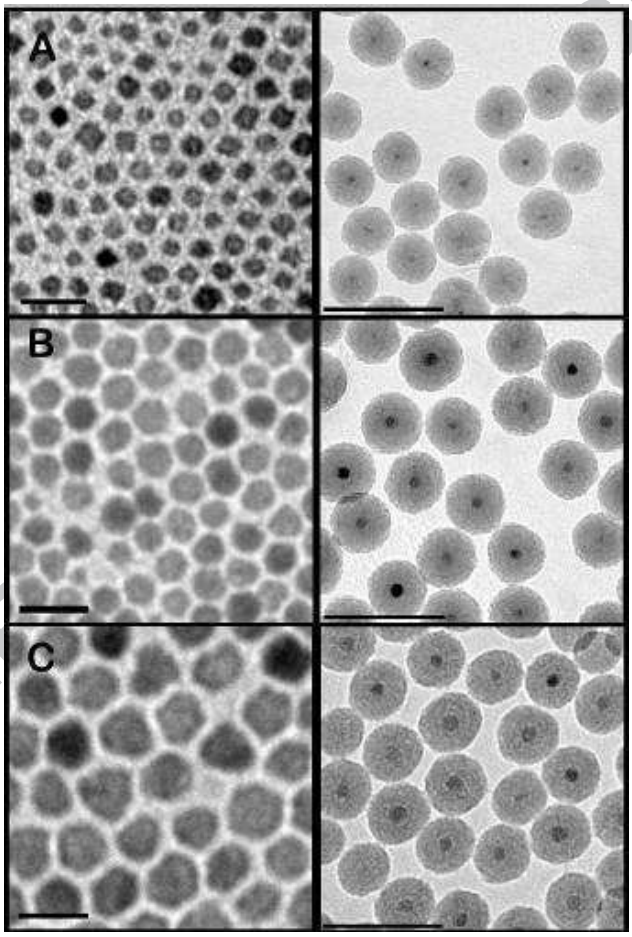

Fig. 1 TEM images of ((a) 6 nm, b) 10.5 nm, c) 15 nm; corresponding scale bar: 20 nm) γ-Fe_2O_3 NPs and the corresponding $[Cs_2Mo_6Br_{14}$-γ-$Fe_2O_3]$@SiO_2 hybrid nanoparticles (scale bar: 100 nm).

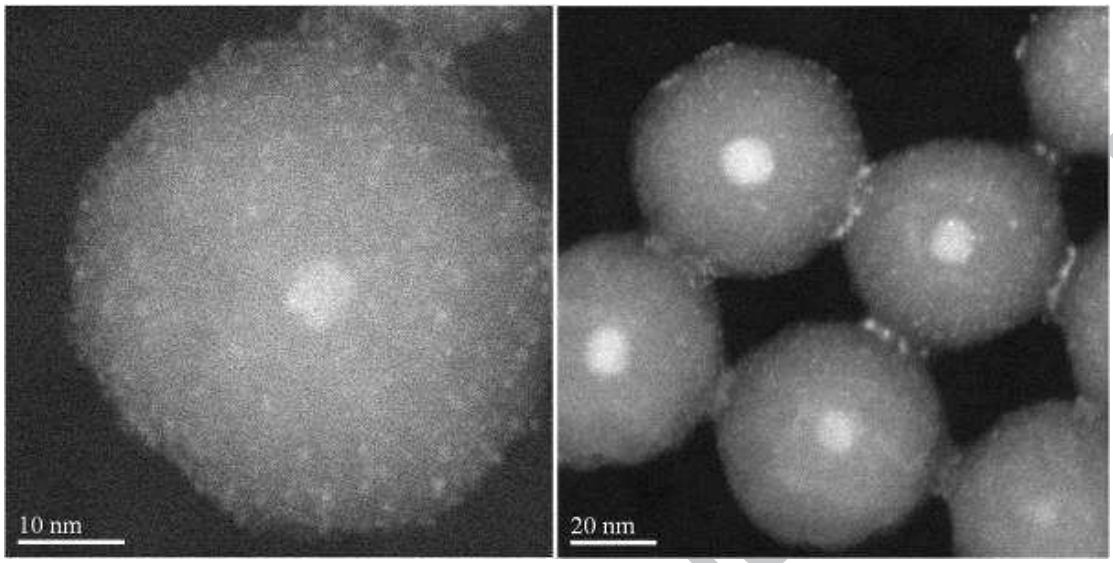

Fig. 2 HAADF-STEM images of $[Cs_2Mo_6Br_{14}\text{-}]Fe_2O_3]@SiO_2$ with magnetic core size of 6 nm (left) and 10.5 nm (right). The cluster units appear as small bright spots.

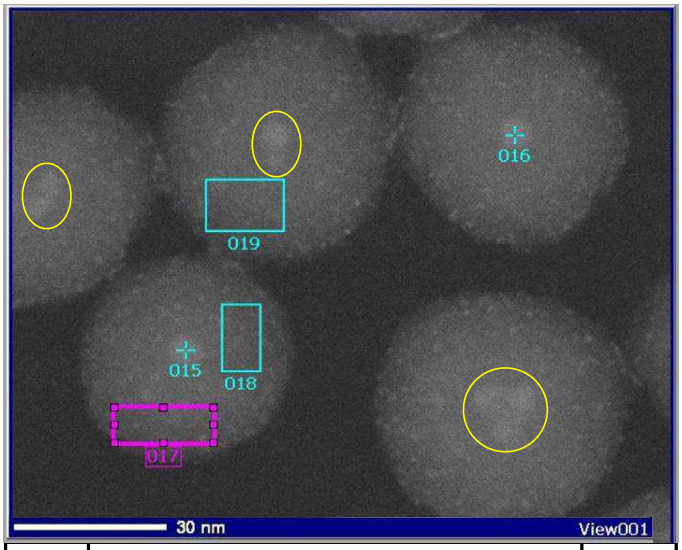

Area	Elements						Atom %
	C	N	O	Si	Fe	Mo	
15	5.68	0	45.57	47.64	0.77	0.35	100
16	2.73	0	50.18	45.65	0.71	0.72	100
17	1	18.66	34.02	45.41	0	0.91	100
18	0.32	0	48.42	50.53	0	0.73	100
19	1.90	8.09	44.14	45.10	0	0.75	100

Fig. 3 EDX elemental analysis realized at different locations of the MLPs. The yellow circles indicate the presence of several magnetic cores in the silica matrix. Size of the magnetic nanoparticles: 6nm.

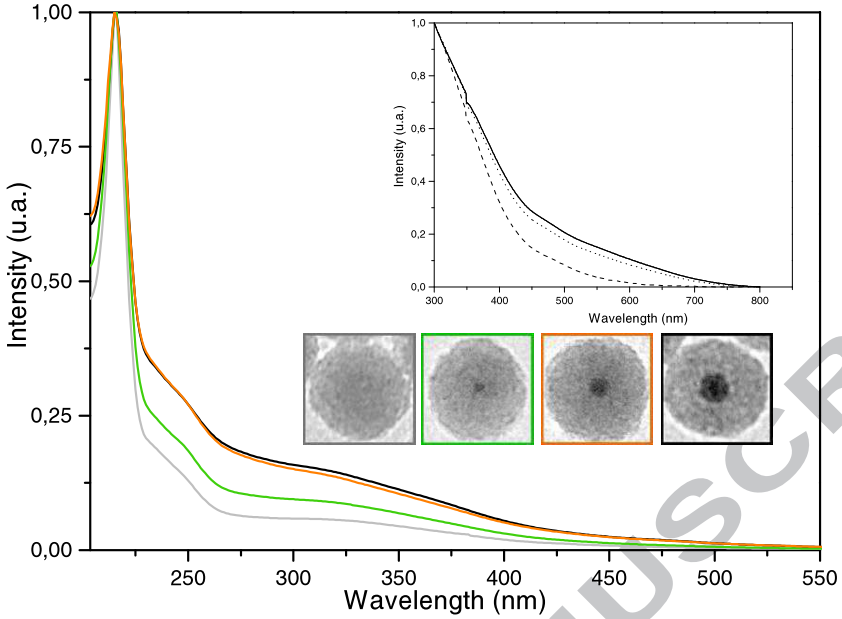

Fig. 4 UV-Vis spectra in water of $[Cs_2Mo_6Br_{14}]@SiO_2$ (gray) and $[Cs_2Mo_6Br_{14}$-$\gamma Fe_2O_3]@SiO_2$ with a magnetic core of 6 (green), 10.5 (orange) and 15 nm (black). Spectra are normalized at 215 nm for comparison. The inset shows the absorption of 6 nm (dash line), 10.5 nm (dot line) and 15 nm (solid line) γ-Fe_2O_3 MPs in cyclohexane.

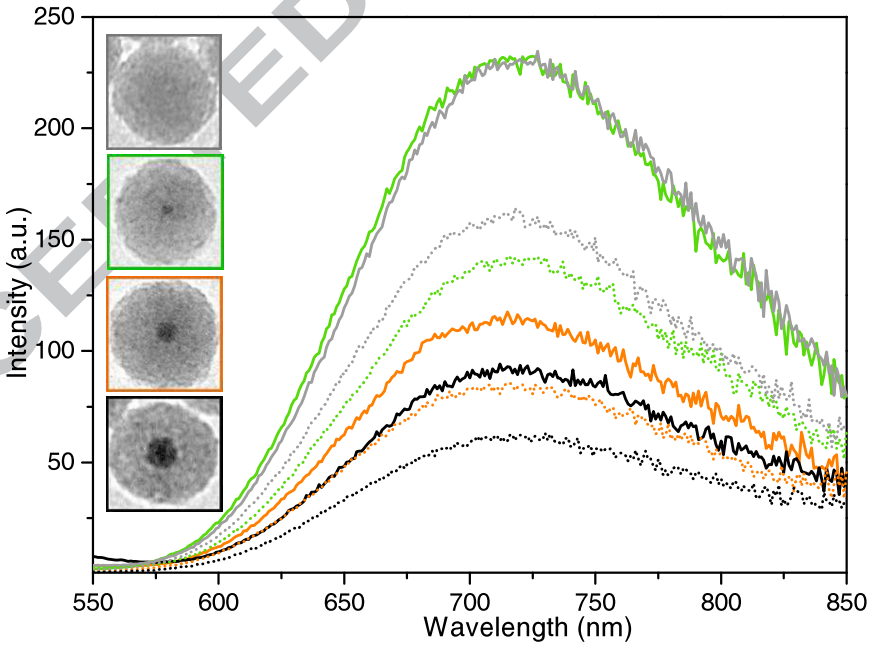

Fig. 5 Emission spectra in water (λ_{exc} = 450 nm) of $[Cs_2Mo_6Br_{14}]@SiO_2$ (gray) and $[Cs_2Mo_6Br_{14}$-$\gamma Fe_2O_3]@SiO_2$ nanoparticles with different core size with (dot

lines) and without (solid lines) oxygen. In order to compare these spectra, all the samples were adjusted to the same concentration of clusters. Luminescent spectra were first recorded under ambient conditions and just after deoxygenated with a flow of argon directly in the optical cells during 2h and spectra were recorded immediately after. After 2h of deoxygenation, intensity remained constant. The experimental setup being the same, the intensity of the emission can be directly compared. Mean diameter of the silica spheres, from top to bottom: 38 (empty), 45, 50 and 53 nm.

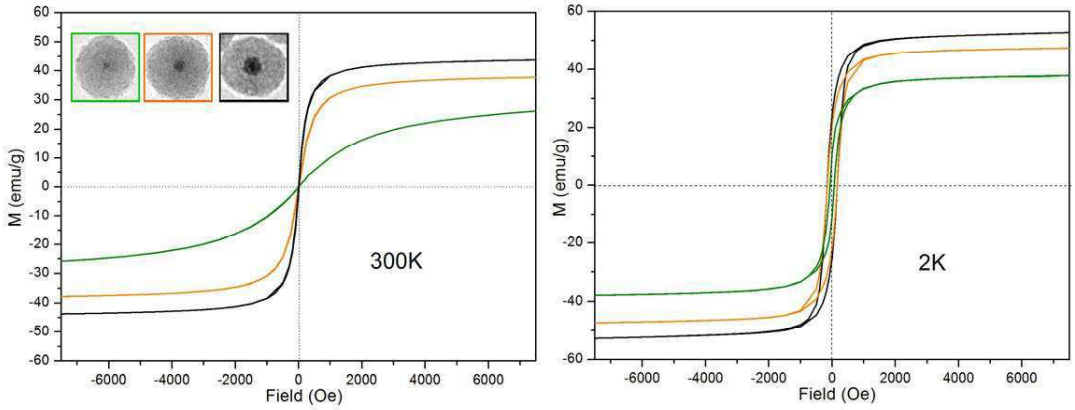

Fig. 6 Magnetic hysteresis loops at 300 K (left) and 2 K (right) of $[Cs_2Mo_6Br_{14}$-$\gamma Fe_2O_3]@SiO_2$ NPs with different magnetic core size. Data were normalized to emu per gram of Fe_2O_3 content.

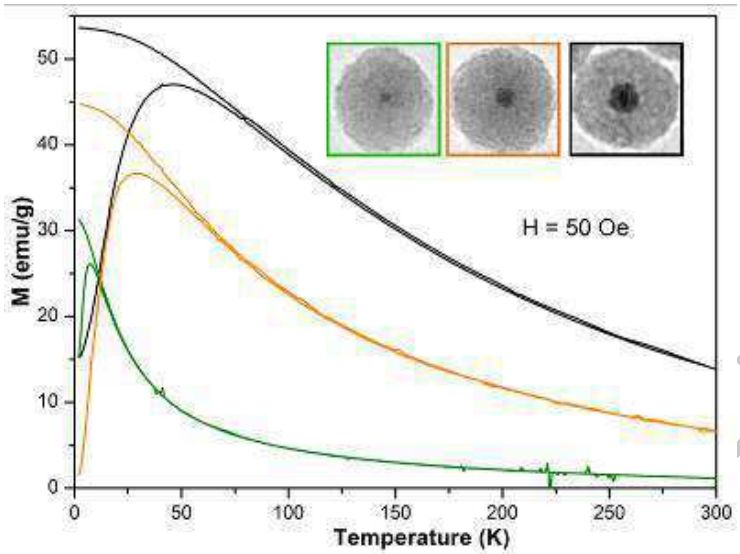

Fig. 7 ZFC and FC curves vs temperature of $[Cs_2Mo_6Br_{14}$-γ$Fe_2O_3]@SiO_2$ nanoparticles.

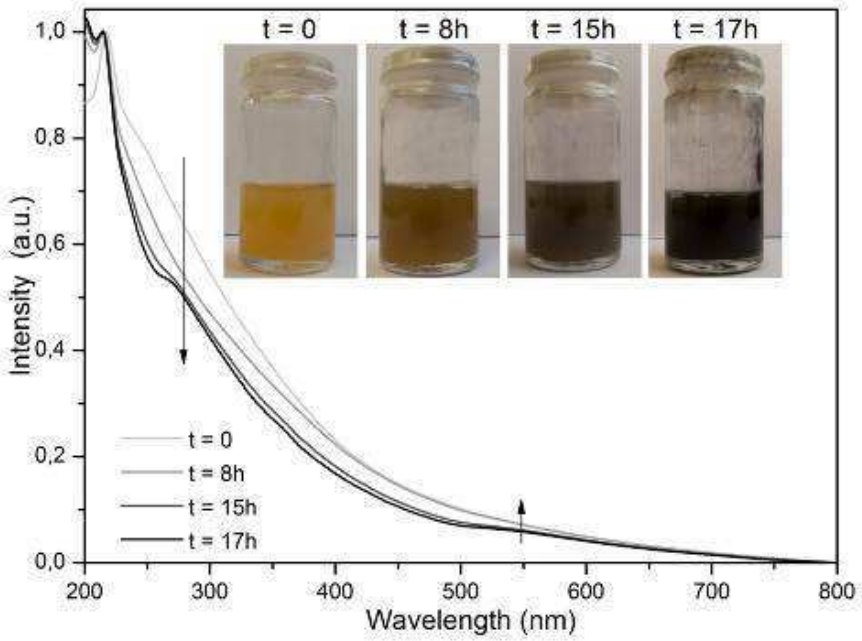

Fig. 8 Evolution in time of the absorbance spectrum of a suspension of ($[Cs_2Mo_6Br_{14}$-γ$Fe_2O_3]@SiO_2$ + $AuCl_4.3H_2O$) under UV irradiation. The color of the suspension changed progressively from yellow to gray-black. The inset shows an enlargement of the plasmon zone, proving the formation of gold nanoparticles.

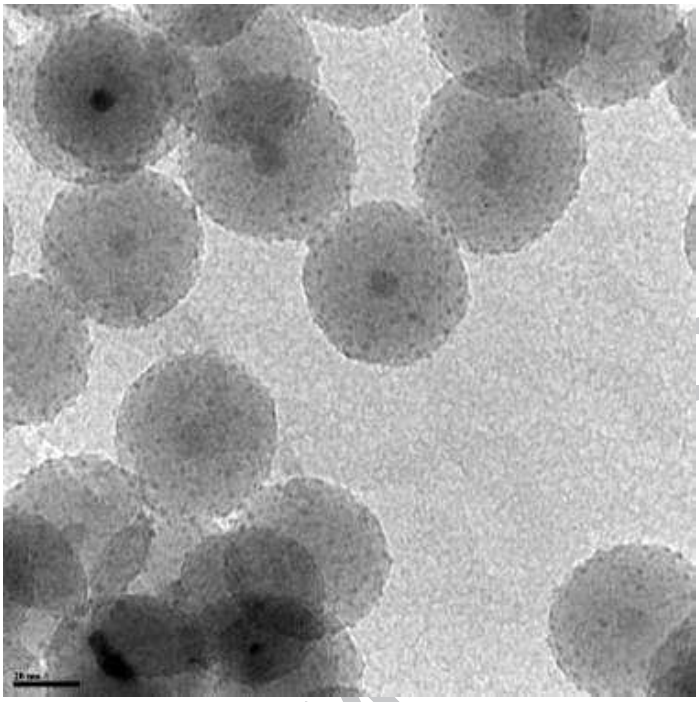

Fig. 9 TEM image of $[Cs_2Mo_6Br_{14}\text{-}\gamma Fe_2O_3]@SiO_2@Au$. Magnetic core size: 10.5 nm. Gold nanoparticles appears as small darker spot.

	Without O_2	With O_2
$[Cs_2Mo_6Br_{14}]@SiO_2$	1	0.7
$[Cs_2Mo_6Br_{14}$-γ$Fe_2O_3]@SiO_2$ **1** core size: 6 nm	1	0,62
$[Cs_2Mo_6Br_{14}$-γ$Fe_2O_3]@SiO_2$ **2** core size: 10.5 nm	0.51	0.38 0.74 if compared to **2** without O_2
$[Cs_2Mo_6Br_{14}$-γ$Fe_2O_3]@SiO_2$ **3** core size: 15 nm	0.42	0.27 0.64 if compared to **3** without O_2

Table 1 Relative luminescence intensity with and without oxygen of $[Cs_2Mo_6Br_{14}]@SiO_2$ and $[Cs_2Mo_6Br_{14}$-γ$Fe_2O_3]@SiO_2$ with the three magnetic core sizes. Intensity of $[Cs_2Mo_6Br_{14}]@SiO_2$ without oxygen was taken as reference. Relative intensities were calculated by integrating the luminescent spectra area between 480 and 850 nm.

	t1 [µs]	A1	t2 [µs]	A2	t3 [µs]	A3
$[Mo_6Br_{14}]@SiO_2$	100	0.083	30	0.463	8.5	0.454
Mo_6Br_{14}-γ$Fe_2O_3]@SiO_2$ core size: 6 nm	90	0.186	30	0.397	10	0.417
$[Mo_6Br_{14}$-γ$Fe_2O_3]@SiO_2$ core size: 10.5 nm	100	0.141	50	0.267	20	0.592
$[Mo_6Br_{14}$-γ$Fe_2O_3]@SiO_2$ core size: 15 nm	100	0.124	30	0.34	10	0.536

Table 2 Photoluminescence lifetime of $[Cs_2Mo_6Br_{14}]@SiO_2$ and $[Cs_2Mo_6Br_{14}$-γ$Fe_2O_3]@SiO_2$ nanoparticles in water (λ_{exc} = 450 nm and λ_{obs} = 700 nm). The kinetic parameters were obtained by fitting the luminescence decay curves with a three exponential equation as followed: $y= A_1e(-x/\tau1) +A_2e(-x/\tau2) + A_3e(-x/\tau3)$. A1, A2 and A3 represent the ponderation coefficient of each exponential. The sum of these coefficients was fixed to 1 to avoid aberrant results.

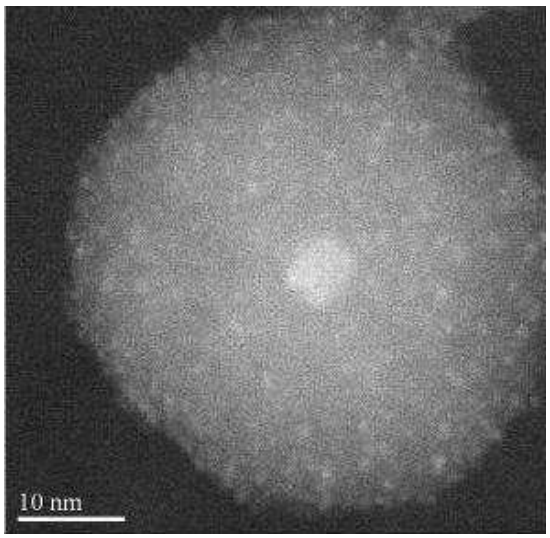

- NIR and superparamagnetic nanoparticles were synthesized by W/O microemulsion process.
- Monodisperse silica nanoparticles with complex architectures and below 50 nm in size
- NIR luminescent nanosized $[Mo_6Br_{14}]^{2-}$ cluster units